AMERICAN SOCIETY FOR MICROBIOLOGY | Journal of Virology®

CELLULAR RESPONSE TO INFECTION

Porcine Reproductive and Respiratory Syndrome Virus Infection Upregulates Negative Immune Regulators and T-Cell Exhaustion Markers

Jayeshbhai Chaudhari,[a,b] Chia-Sin Liew,[c] Jean-Jack M. Riethoven,[c,d,e] Sarah Sillman,[b] Hiep L. X. Vu[a,f]

[a]Nebraska Center for Virology, University of Nebraska-Lincoln, Lincoln, Nebraska, USA
[b]School of Veterinary Medicine and Biomedical Sciences, University of Nebraska-Lincoln, Lincoln, Nebraska, USA
[c]Center for Biotechnology, University of Nebraska-Lincoln, Lincoln, Nebraska, USA
[d]Nebraska Center for Integrated Biomolecular Communication, University of Nebraska-Lincoln, Lincoln, Nebraska, USA
[e]Department of Biochemistry, University of Nebraska-Lincoln, Lincoln, Nebraska, USA
[f]Department of Animal Science, University of Nebraska-Lincoln, Lincoln, Nebraska, USA

ABSTRACT Porcine alveolar macrophage (PAM) is one of the primary cellular targets for porcine reproductive and respiratory syndrome virus (PRRSV), but less than 2% of PAMs are infected with the virus during the acute stage of infection. To comparatively analyze the host transcriptional response between PRRSV-infected PAMs and bystander PAMs that remained uninfected but were exposed to the inflammatory milieu of an infected lung, pigs were infected with a PRRSV strain expressing green fluorescent protein (PRRSV-GFP), and GFP^+ (PRRSV infected) and GFP^- (bystander) cells were sorted for RNA sequencing (RNA-seq). Approximately 4.2% of RNA reads from GFP^+ and 0.06% reads from GFP^- PAMs mapped to the PRRSV genome, indicating that PRRSV-infected PAMs were effectively separated from bystander PAMs. Further analysis revealed that inflammatory cytokines, interferon-stimulated genes, and antiviral genes were highly upregulated in GFP^+ compared to GFP^- PAMs. Importantly, negative immune regulators, including NF-κB inhibitors (NFKBIA, NFKBID, NFKBIZ, and TNFAIP3) and T-cell exhaustion markers (programmed death ligand-1 [PD-L1], PD-L2, interleukin-10 [IL-10], IDO1, and transforming growth factor β2 [TGFB2]) were highly upregulated in GFP^+ cells compared to GFP^- cells. By using an *in situ* hybridization assay, RNA transcripts of tumor necrosis factor (TNF) and NF-κB inhibitors were detected in PRRSV-infected PAMs cultured *ex vivo* and lung sections of PRRSV-infected pigs during the acute stage of infection. Collectively, the results suggest that PRRSV infection upregulates expression of negative immune regulators and T-cell exhaustion markers in PAMs to modulate the host immune response. Our findings provide further insight into PRRSV immunopathogenesis.

IMPORTANCE Porcine reproductive and respiratory syndrome virus (PRRSV) is widespread in many swine-producing countries, causing substantial economic losses to the swine industry. Porcine alveolar macrophage (PAM) is considered the primary target for PRRSV replication in pigs. However, less than 2% of PAMs from acutely infected pigs are infected with the virus. In the present study, we utilized a PRRSV strain expressing green fluorescent protein to infect pigs and sorted infected and bystander PAMs from the pigs during the acute stage of infection for transcriptome analysis. PRRSV-infected PAMs showed a distinctive gene expression profile and contained many uniquely activated pathways compared to bystander PAMs. Interestingly, upregulated expression of NF-κB signaling inhibitors and T-cell exhaustion molecules were observed in PRRSV-infected PAMs. Our findings provide additional knowledge on the mechanisms that PRRSV employs to modulate the host immune system.

KEYWORDS PRRSV, transcriptome, RNA-seq, NF-κB inhibitors, T-cell exhaustion, NF-κB inhibitors

Citation Chaudhari J, Liew C-S, Riethoven J-JM, Sillman S, Vu HLX. 2021. Porcine reproductive and respiratory syndrome virus infection upregulates negative immune regulators and T-cell exhaustion markers. J Virol 95:e01052-21. https://doi.org/10.1128/JVI.01052-21.

Editor Tom Gallagher, Loyola University Chicago

Address correspondence to Hiep L. X. Vu, hiepvu@unl.edu.

Received 23 June 2021
Accepted 5 August 2021
Accepted manuscript posted online 11 August 2021
Published 13 October 2021

Porcine reproductive and respiratory syndrome virus (PRRSV) is a major swine viral pathogen that is currently circulating in many swine-producing countries. It is an enveloped, positive-sense, and single-stranded RNA virus belonging to the order *Nidovirales*, family *Arteriviridae*, and genus *Portarterivirus* with a genome of approximately 15 kb. According to the recently updated taxonomy, PRRSV is classified into two distinct species: *Betaarterivirus suid 1* (previously known as PRRSV-1) and *Betaarterivirus suid 2* (previously known as PRRSV-2) (1). The virus is known to infect only swine. It has a restricted tropism for the cells of monocytic lineages (2). Viral antigen can be detected in lung and various lymphoid tissues, including tonsil, spleen, and lymph nodes (2). Porcine alveolar macrophage (PAM) is considered the major target for PRRSV infection, and no more than 2% of lung alveolar macrophages are infected with the virus (2).

PRRSV infection of pigs induces poor innate and adaptive immune responses. Several mechanisms for PRRSV-mediated immune suppression have been reported, which includes the modulation of crucial immune signaling pathways such as NF-κB, retinoic acid-inducible gene I (RIG-I), and Janus kinase/signal transducer and activator of transcription (JAK-STAT) (3–6). The ovarian tumor (OTU) domain within the viral nonstructural protein (nsp) 2 possesses ubiquitin-deconjugating activity which inhibits NF-κB activation by preventing the polyubiquitination and proteasomal degradation of IκBα, an inhibitor of the NF-κB pathway (3). Nsp1α and nsp1β suppress tumor necrosis factor-α (TNF-α) induction by modulating the NF-κB and AP1 element binding sites, respectively, on the TNF-α promoter (7). Similarly, the viral nucleocapsid (N) protein upregulates expression of suppressor of cytokine signaling 1 (SOCS1), a negative regulator that suppresses interferon-stimulated gene (ISG) activation, to support PRRSV replication (8). Furthermore, some strains of PRRSV were reported to induce expression of T-cell exhaustion marker programmed death ligand-1 (PD-L1) (CD274) in monocyte-derived dendritic cells, suggesting that the virus might be able to modulate the host T-cell response (9).

Many transcriptomic studies have been conducted to elucidate the host responses to PRRSV infection. These studies have been performed using different types of tissues, including peripheral blood mononuclear cells, lung alveolar macrophages, parenchymal mononuclear phagocytes, lung tissue, and tracheobronchial lymph node, that were collected from pigs infected with different PRRSV strains (10–14). Additionally, several studies have been conducted using PRRSV-infected PAMs that were cultured *ex vivo* (15–17). The results of these studies are highly heterogeneous. However, most of the studies involving highly pathogenic PRRSV strains reported the upregulation of multiple proinflammatory cytokines (interleukin-8 [IL-8], TNF-α) and chemokine genes (CXCL10, CCR5, CCL4, and CCL2) (11, 15). In a meta-analysis of available gene expression data sets involving PRRSV infection, it was found that TREM1 signaling, role of hypercytokinemia/hyperchemokinemia in the pathogenesis of influenza and Toll-like receptor signaling were the commonly activated pathways in PRRSV infection (18). Particularly, this study reported that upregulation of several chemokines (CCL2, CCL3, CCL4, and CCL5), interleukins (IL-1A, IL-1B, IL-8 and IL-18) and the chemokine receptor 1 (CCR1) were commonly observed among the data sets (18). In these studies, RNA was extracted from the whole population of cells or tissues collected from infected pigs. Since only a small percentage of those cells are infected with the virus (2), the transcriptome responses detected in those studies do not reflect the responses of cells directly infected with PRRSV. Instead, these studies reveal the combined responses from both infected and bystander cells.

The primary objective of this study was to comparatively analyze the transcriptomic response of infected- and bystander- PAMs that were collected from pigs during an acute infection with PRRSV. Pigs were infected with a recombinant PRRSV strain expressing green fluorescent protein (FL12-GFP). At 7 days postinfection (dpi), GFP$^+$ (PRRSV-infected) and GFP$^-$ (bystanders) PAMs were sorted for RNA sequencing (RNA-seq). Many differentially expressed genes (DEGs) and pathways were observed in GFP$^+$ compared to GFP$^-$ cells. Pathways involved in host immune responses against viral infections were highly enriched in both GFP$^+$ and GFP$^-$ PAMs. However, upregulation of negative immune

regulators like NF-κB inhibitors (NFKBIs) and T-cell exhaustion markers were observed only in GFP$^+$ PAMs. Collectively, this study provides new insight into the mechanisms that PRRSV uses to modulate the host immune response.

RESULTS

Isolation of PRRSV-infected and bystander CD163$^+$ PAMs for RNA-seq. A pilot experiment was conducted to determine the kinetics and frequencies of PAMs collected from PRRSV-infected pigs that harbored viral antigens. Twelve weaned pigs were inoculated intramuscularly with a virulent PRRSV strain, FL12, and bronchoalveolar lavage fluid (BALF) was collected at different time points postinfection to analyze for the frequencies of CD163$^+$ PRRSV$^+$ cells by flow cytometry (Fig. 1A). While over 90% of cells from the BALF expressed CD163, the main cellular receptor for PRRSV infection (19), only a small fraction of these cells was infected with PRRSV. Specifically, the mean frequencies of CD163$^+$ PRRSV$^+$ cells were 0.06% at 1 dpi, 0.33% at 3 dpi, and 0.51% at 8 dpi (Fig. 1B). Interestingly, the frequency of CD163$^+$ PRRSV$^+$ cells decreased to undetectable levels at 15 dpi even though the pigs were still viremic at this time point (Fig. 1C).

In the pilot experiment, PAMs were fixed, permeabilized, and stained with PRRSV anti-N protein antibody in order to determine the frequencies of PRRSV-infected cells by flow cytometry. To facilitate the isolation of live cells for RNA-seq, in the second experiment, pigs were inoculated with the PRRSV strain FL12-GFP. BALF was collected at 7 dpi, and CD163$^+$GFP$^+$ cells and CD163$^+$GFP$^-$ cells were sorted by fluorescence-activated cell sorting (FACS) (Fig. 1D). The frequencies of CD163$^+$GFP$^+$ cells were greatly variable among the three PRRSV-infected pigs, ranging from 0.1% to 1% (Fig. 1E), even though they displayed similar levels of serum viral loads (Fig. 1F).

We noted that pigs infected with FL12-GFP exhibited similar frequencies of virus-infected PAMs (Fig. 1B and E) and levels of serum viral loads (Fig. 1C and F) compared to those infected with FL12. Moreover, microscopic lung lesion was similar between pigs infected with FL12-GFP and those infected with FL12 (data not shown). Together, the data suggest that FL12-GFP had a virulence property similar to that of its parental strain, FL12.

RNA-seq data quality and detection of viral transcripts in PRRSV-infected and bystander PAMs. A total of nine cell populations were subjected to RNA-seq—three CD163$^+$ PAMs collected from mock-infected pigs and three CD163$^+$GFP$^+$ and three CD163$^+$GFP$^-$ PAMs collected from FL12-GFP-infected pigs at 7 dpi. The number of RNA reads per sample varied from 34 million to 58 million, with an average of 36 million (Table 1). To determine whether PRRSV-infected PAMs were effectively sorted from the BALF collected from PRRSV-infected pigs, RNA reads were mapped to the FL12-GFP genome. As expected, viral RNA reads were not detected from PAMs collected from mock-infected pigs. On average, 4.2% of RNA reads from GFP$^+$ PAMs and 0.06% of reads from GFP$^-$ PAMs mapped to the FL12-GFP genome (Table 1). Viral reads from GFP$^+$ samples mapped predominantly to the 3′ end of the genome (Fig. 2). The results clearly indicate that PRRSV-infected cells were effectively separated from bystanders.

PRRSV-infected and bystander PAMs display a distinct transcriptome profile. To examine the host responses to PRRSV infection, RNA reads were mapped to the reference pig genome (Sscrofa11.1; GenBank assembly number GCF_000003025.6). A total of 25,394 pig genes were identified in this study. Principal-component analysis (PCA) revealed that the three PAM populations were segregated by their infection status (Fig. 3A). This finding demonstrated that PAMs directly infected with PRRSV have distinct transcriptional profiles compared to the bystander PAMs that remained uninfected but were exposed to the inflammatory milieu of an infected lung.

DEGs were first determined by comparing the relative abundance of transcripts between mock-infected and GFP$^+$ PAMs (mock versus GFP$^+$) and between mock-infected and GFP$^-$ PAMs (mock versus GFP$^-$). The mock versus GFP$^-$ comparison revealed 198 DEGs—164 upregulated and 34 downregulated genes (Fig. 3B). The top 25 upregulated DEGs in this comparison included interferon-stimulated genes [ISG12(A), ISG20, GBP1, GBP2, STAT1, GVIN1, RTP4, NMI, and PARP9], negative regulators of cellular signaling

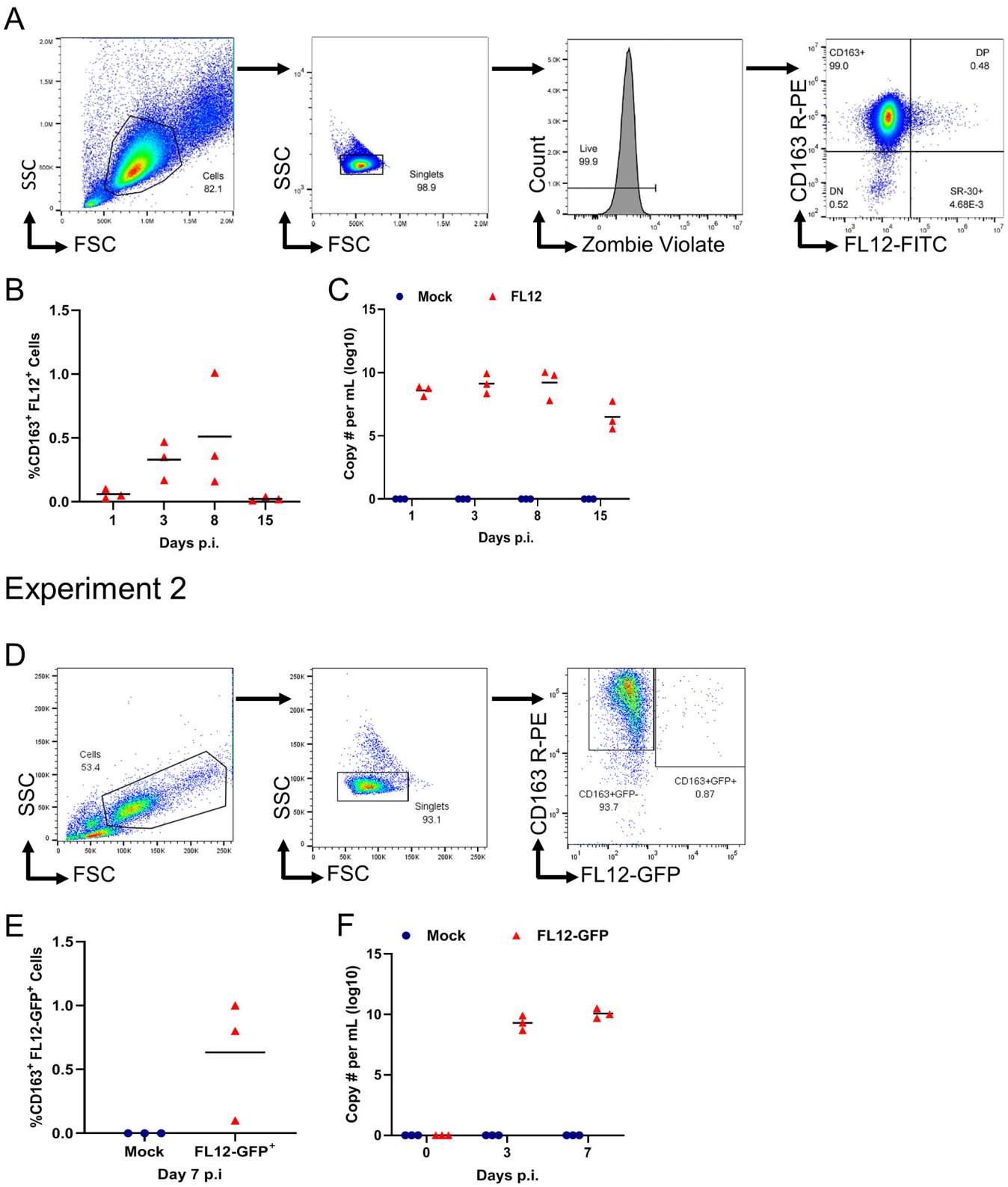

FIG 1 Frequencies of PRRSV-infected PAMs from pigs during the acute stage of infection and sorting of PRRSV-infected and bystander PAMs. (Experiment 1) To determine the kinetics of PRRSV-infection in PAM, 12 pigs were inoculated intramuscularly with PRRSV strain FL12. At different days postinfection (p.i.), PAMs were collected and stained for porcine CD163 receptor and anti-PRRSV N protein. (A) Representative flow cytometry plots showing the gating

(Continued on next page)

TABLE 1 Summary of sequencing quality control and read mapping statistics

Sample name	Total no. of reads	Total no. of quality trimmed reads	Total mapped reads	Total no. of uniquely mapped reads	Uniquely mapped reads (%)	No. of viral reads	Viral reads (%)
Mock 500H	57,549,647	57,352,945	55,491,701	53,680,312	93.6	1,427	0.0
Mock 501B	58,263,397	58,071,152	56,202,005	54,359,509	93.6	485	0.0
Mock 501C	44,666,037	44,505,522	43,012,952	41,698,476	93.7	295	0.0
GFP$^-$ 500B	47,334,964	47,168,580	45,597,702	44,056,250	93.4	26,961	0.1
GFP$^-$ 503A	56,372,523	56,159,073	54,369,701	52,601,975	93.7	30,017	0.1
GFP$^-$ 598E	36,394,100	36,266,288	35,098,482	33,927,222	93.5	694	0.0
GFP$^+$ 500B	47,011,665	46,844,364	42,808,562	41,190,157	87.9	2,275,791	4.9
GFP$^+$ 503A	50,040,720	49,853,736	45,326,169	43,765,943	87.8	2,560,535	5.1
GFP$^+$ 598E	34,027,315	33,875,247	31,816,789	30,865,285	91.1	926,100	2.7

(DUSP10 and ACKR2), mitophagy receptor (FUNDC1), and other cellular signaling molecules (UBD, SASH1, C3AR1, CASP1, and ERAP2). The top 25 downregulated genes mainly involved in induction of inflammatory responses (FSTL1, RAI14, PPBP, KLF12, MFGE8, and MARCO). The results indicate that the GFP$^-$ PAMs collected from FL12-GFP-infected pigs had distinct transcriptional profiles compared to PAMs collected from mock-infected pigs. Thus, the GFP$^-$ PAMs were regarded as bystander cells in this study.

The degree of transcriptional change was more profound in the GFP$^+$ PAMs than in the GFP$^-$ PAMs. In particular, the mock versus GFP$^+$ comparison revealed 1,072 DEGs–910 upregulated and 162 downregulated genes (Fig. 3C). The top 25 upregulated genes in this comparison included several inflammatory cytokines (IL-1B, IL-1A, and TNF), chemokines (CCL4 and CCL3L1), interferon-stimulated genes (GBP1, GBP2, IRF1, and IFIH1), and type-I interferons (IFNB1, IFN-Alphaomega). Notably, NFKBIA, a negative feedback regulator of the NF-κB signaling pathway (20), was also among the top 25 upregulated genes in the mock versus GFP$^+$ comparison (Fig. 3C). Genes that were downregulated were mostly associated with cell adhesion (MFGE8, ITGB5, SPN, and CDH24), cell growth regulation (MAMDC2, LSAMP, TESK2, MXD3, SESN3, and CDCA72), and cell metabolism (PYGL and HILPDA) (Fig. 3C).

The majority of DEGs found in the mock versus GFP$^-$ comparison were also found in the mock versus GFP$^+$ comparison (Fig. 3D). Thus, direct comparison of the relative transcript abundance between GFP$^+$ and GFP$^-$ PAMs (GFP$^+$ versus GFP$^-$ comparison) was performed to identify genes that were affected by direct PRRSV infection. Compared with GFP$^-$, the GFP$^+$ PAMs had 338 DEGs (Fig. 3E), several of which are proinflammatory genes such as TNF, IL-1A, IL-1B, CCL4, and CXCL2. Interestingly, several anti-inflammatory genes, including the negative regulators of NF-κB, such as NFKBIA and NFKBIZ (Fig. 3E), were also upregulated in GFP$^+$ PAMs relative to GFP$^-$ PAMs. There were only 4 downregulated DEGs in the GFP$^-$ versus GFP$^+$ comparison, METTL24, SPN, TP53INP1, and SMPD5.

Canonical pathway enrichment analysis between PRRSV-infected and bystander PAMs. The total DEGs identified from the three pairwise comparisons, namely, mock versus GFP$^+$, mock versus GFP$^-$, and GFP$^-$ versus GFP$^+$, were analyzed by Ingenuity pathway analysis (IPA) to identify canonical cellular pathways that were enriched in each comparison. Pathways commonly activated in both the mock versus GFP$^+$ and mock versus GFP$^-$ comparisons included systemic lupus erythematosus in B cell signaling, neuroinflammation signaling, retinoic acid-mediated apoptosis, interferon signaling, and role of pattern recognition receptors in recognitions of bacteria and viruses (Fig. 4A). These pathways are highly interconnected and involved in the antiviral

FIG 1 Legend (Continued)
strategy used to determine the percentage of PAM infected with PRRSV. (B) Percentage of CD163$^+$FL12$^+$ cells at 1, 3, 8, and 15 dpi. (C) Viral loads in serum determined by qRT-PCR. (Experiment 2) To isolate PRRSV-infected and bystander PAMs, pigs were inoculated with PRRSV strain FL12-GFP. At 7 dpi, PAMs were harvested and sorted from both PRRSV-infected (CD163$^+$GFP$^+$) and bystander (CD163$^+$GFP$^-$) cells. (D) Representative gating strategy used to sort CD163$^+$GFP$^+$ (infected) and CD163$^+$GFP$^-$ (bystander) PAMs for the RNA-seq study. (E) Percentage of PAMs infected with FL12-GFP strain at 7 dpi. (F) Viral loads in serum determined by qRT-PCR.

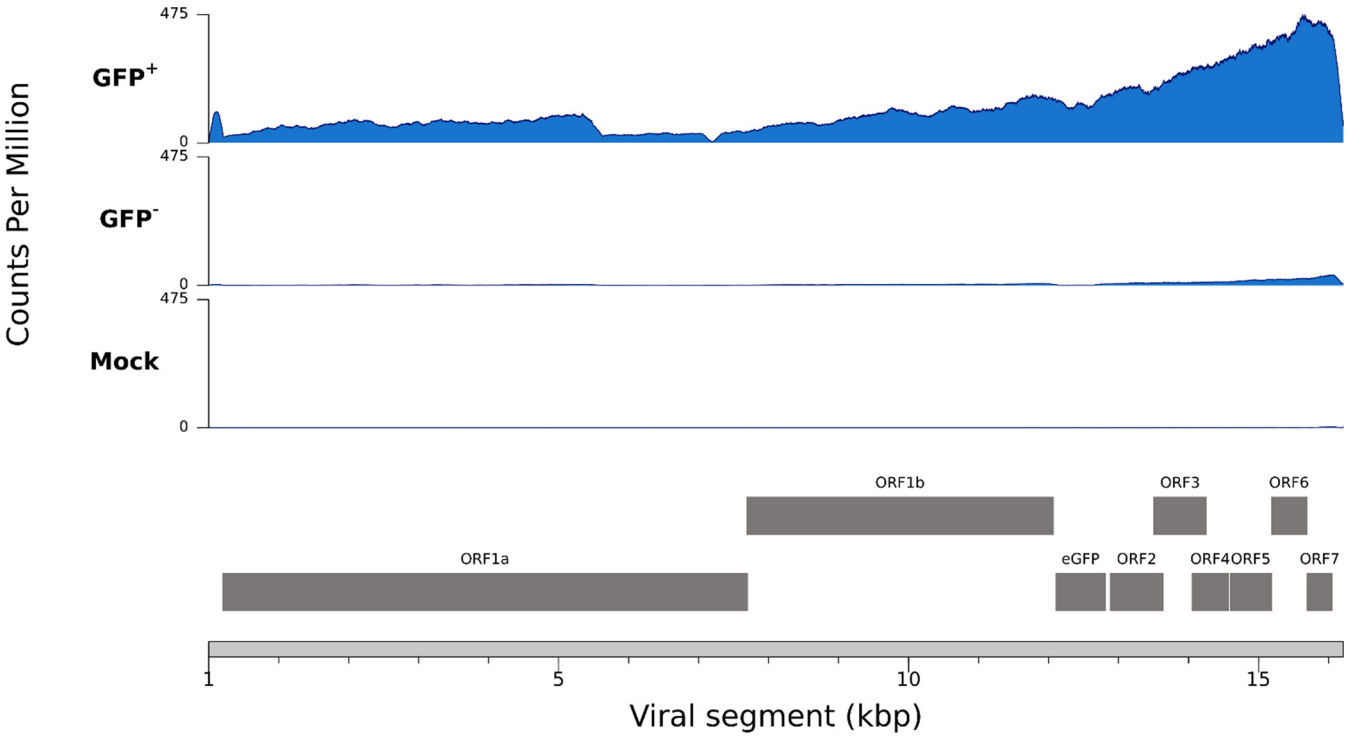

FIG 2 Coverage plot of the RNA reads mapped to the FL12-GFP genome. The *y* axis represents the count per million, while the *x* axis represents the viral genome. Gray boxes under the plot depict the locations of PRRSV open reading frames.

immune responses. Notable pathways that were only activated in the mock versus GFP$^+$ and/or GFP$^-$ versus GFP$^+$ comparisons included T-cell exhaustion signaling, dendritic cell maturation, high mobility group box 1 (HMGB1) signaling, IL-15 signaling, triggering receptor expressed on myeloid cells 1 (TREM-1) signaling, and NF-κB signaling (Fig. 4B). The coronavirus pathogenesis pathway was the only pathway that was commonly inactivated in both the mock versus GFP$^+$ and mock versus GFP$^-$ comparisons (Fig. 4C). Finally, the canonical pathways that were selectively inactivated in the mock versus GFP$^+$ and/or GFP$^-$ versus GFP$^+$ comparison included peroxisome proliferator-activated receptor (PPAR) signaling, antioxidant activation of vitamin C, liver X receptor/retinoid X receptor (LXR/RXR) activation, lipopolysaccharide (LPS)/IL-1-mediated inhibition of RXR function, and CD40 signaling (Fig. 4C).

Most of the enriched pathways identified in this study were also reported in a previous study with *ex vivo* infection of PAMs (15). Notably, activation of T-cell exhaustion, NF-κB signaling, and NF-κB activation by viruses, which largely comprise negative regulators of inflammatory responses, are only observed in GFP$^+$, not in GFP$^-$ PAMs (Fig. 4B). Therefore, we will discuss in more detail in the following sections the DEGs involved in these pathways and their possible roles during an acute viral infection.

NF-κB inhibitors were selectively upregulated in PRRSV-infected PAMs. NF-κB is an inducible transcription factor that regulates various cell physiological functions that mediate cell survival, inflammatory response, and immune responses (20). Several genes involved in the NF-κB pathway were only upregulated in the GFP$^-$ versus GFP$^+$ comparison (Fig. 5A). These included inflammatory genes that are activated by NF-κB, such as IFNB1, CCL20, CCL4, TNF, IL-1B, CXCL8, IL-1A, and CCL5 (Fig. 5B). Interestingly, several negative regulators of NF-κB were also upregulated in the GFP$^-$ versus GFP$^+$ comparison, including NFKBIA, NFKBID, NFKBIZ, and TNF-α-induced protein 3 [TNFAIP3] (Fig. 5C). Additionally, suppressors of cytokine signaling molecules (SOCS1 and SOCS3) were also upregulated in the GFP$^+$ cells.

Detection of TNF and NFKBIs transcripts in PAMs infected with PRRSV *ex vivo*. *In situ* hybridization (ISH) was used to analyze the expression of PRRSV and 4 selected host

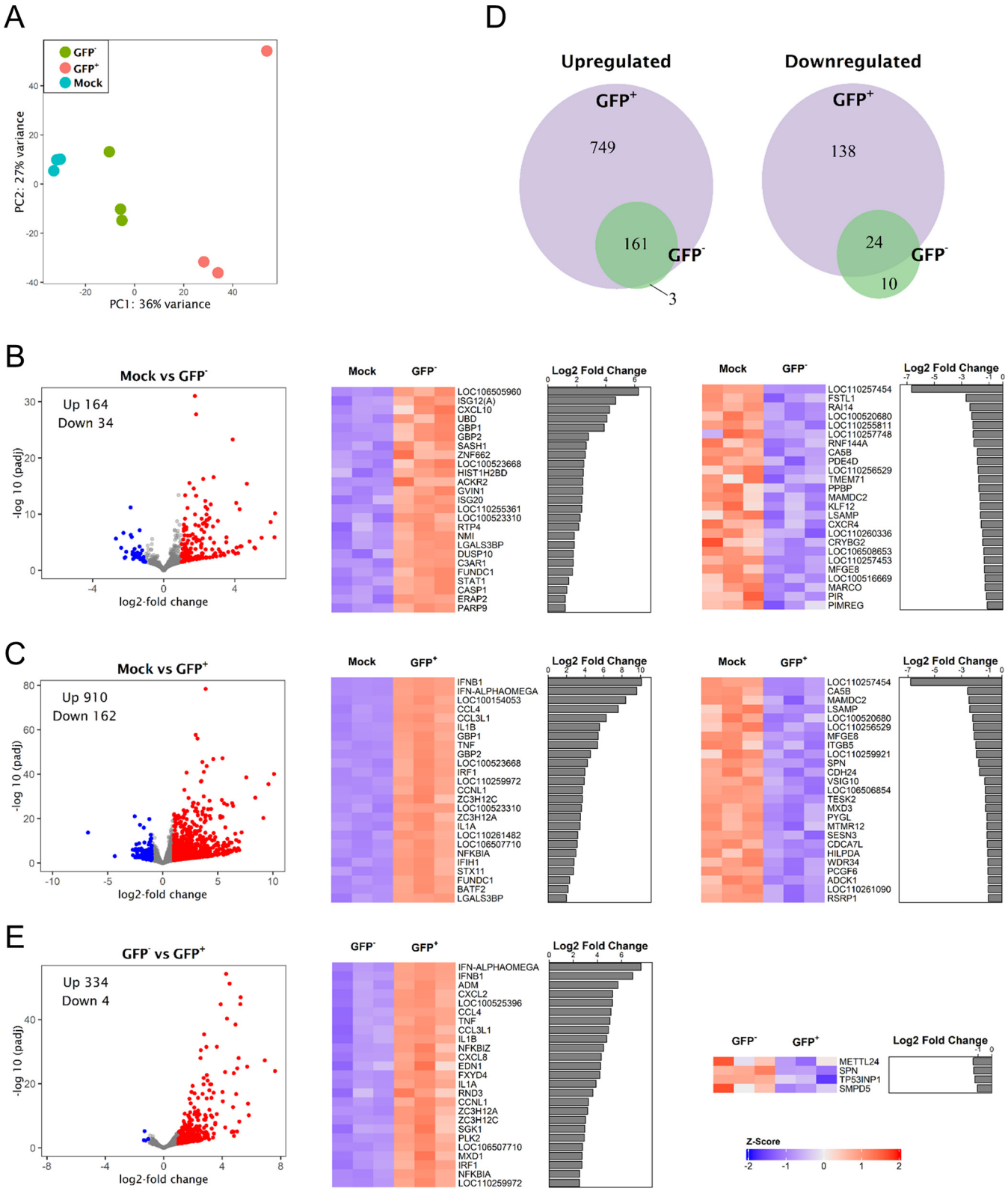

FIG 3 PRRSV infection induces profound transcriptomic changes. (A) Principal-component analysis score plot. Values on each axis (principal component 1 [PC1 and PC2] represent the percentage of variance explained by each component. (B, C, and E) Volcano plots of differentially expressing host genes (adjusted *P* value of <0.05 and $|\text{Log2FC}| > 1$) with the heatmap of top the 25 upregulated or downregulated genes from three different pairwise comparisons are shown. In the volcano plots, red dots represent the upregulated genes, whereas blue dots or boxes represent the downregulated genes. Bar graphs show the $\log_2$ fold change of the top upregulated and downregulated transcripts from each comparison. (D) Venn diagrams showing overlapping DEGs between two pairwise comparisons—mock versus GFP$^+$ and mock versus GFP$^-$.

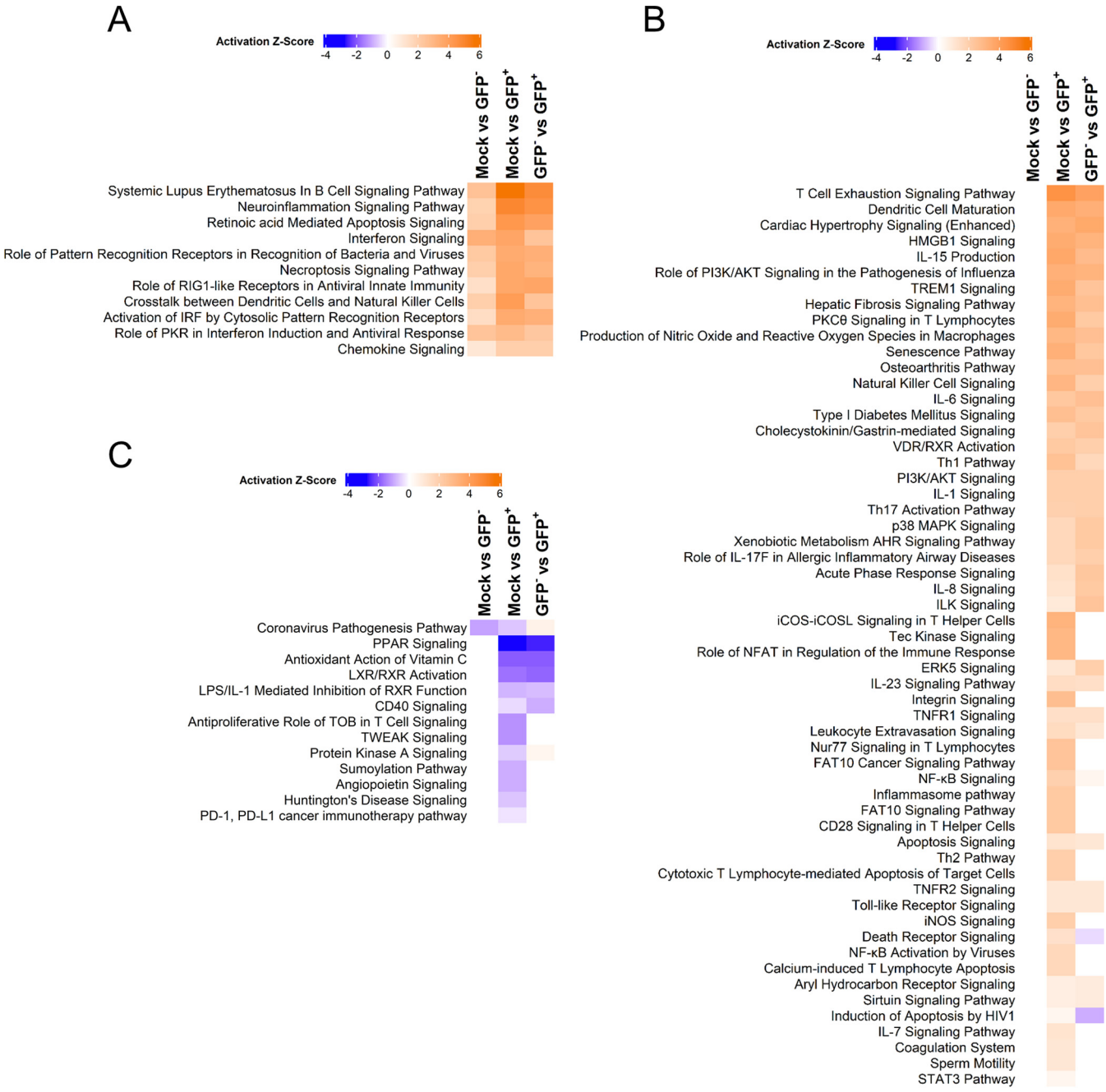

FIG 4 Top canonical signaling pathways modulated by PRRSV infection in PAMs. Total DEGs identified from the three pairwise comparisons; mock versus GFP$^+$, mock versus GFP$^-$, and GFP$^-$ versus GFP$^+$ were analyzed by IPA to identify canonical cellular pathways that were enriched in each of these comparisons. Blue and orange colors represent negative and positive Z-scores, respectively, indicating that the biological pathway is activated or suppressed based on the DEGs detected in each comparison. (A) Canonical signaling pathways commonly activated in all three pairwise comparisons. (B) Canonical signaling pathways only activated in the mock versus GFP$^+$ and/or GFP$^-$ versus GFP$^+$ comparison. (C) All inactivated canonical signaling pathways from all three pairwise comparisons.

genes, NFKBIA, NFKBIZ, TNFAIP3, and TNF, in PAMs infected with PRRSV *ex vivo*. PRRSV-infected cells were detected early at 6 h postinfection (hpi), and the frequency of PRRSV$^+$ cells increased significantly at 18 hpi (Fig. 6). Similarly, the expression of the four selected host genes, NFKBIA, NFKBIZ, TNFAIP3, and TNF, was also detected at 6 hpi and increased significantly at 18 hpi. Of the 4 host genes analyzed, expression of NFKBIA, NFKBIZ, and TNFAIP3 was more profound than that of TNF at 18 hpi (Fig. 6). Collectively, these data support the *in vivo* observations that PRRSV infection upregulates NF-κB inhibitors.

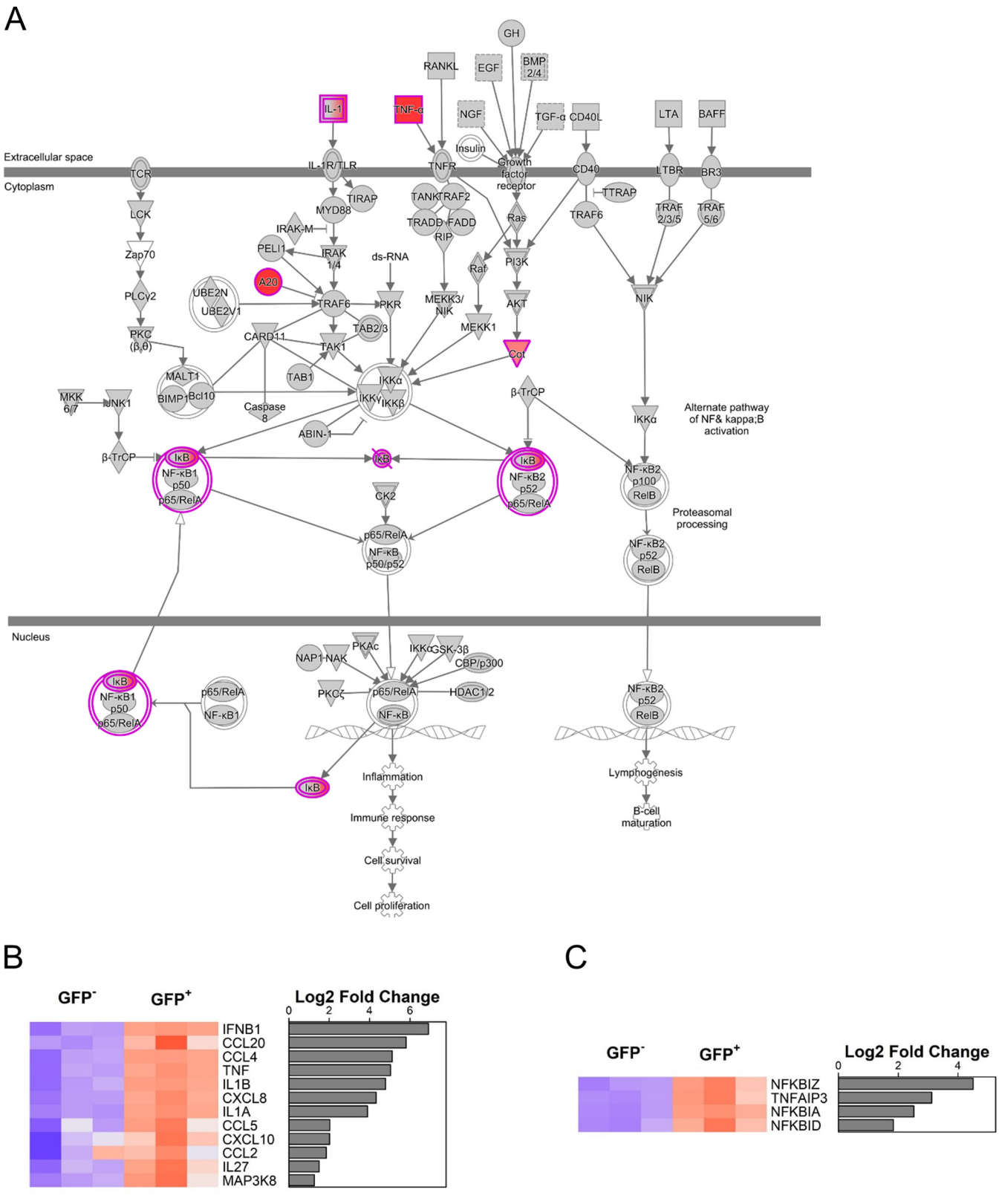

FIG 5 Upregulation of both pro- and anti-inflammatory signals in GFP$^+$ cells. (A) Pathway image from IPA illustrating genes associated in the NF-κB signaling pathway using DEGs from the GFP$^-$ versus GFP$^+$ comparison. Red color indicates the genes that are upregulated in this study. Nondifferentially expressed genes within the pathway are depicted in gray. (B) Heatmap showing the inflammatory genes regulated by the NF-κB signaling pathway and differentially expressed from the GFP $^-$ versus GFP$^+$ comparison. (C) Heatmap showing the upregulation of negative feedback regulators of the NF-κB signaling pathway from the GFP $^-$ versus GFP$^+$ comparison. Bar graphs show the $\log_2$ fold change of the differentially expressed genes.

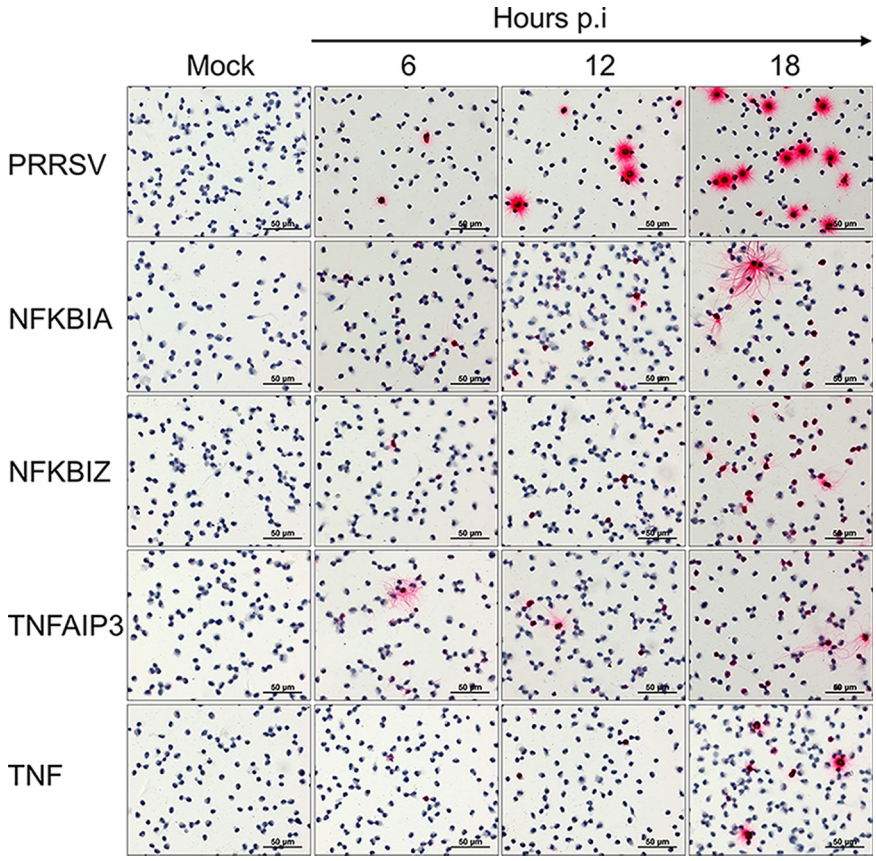

FIG 6 Detection of RNA transcripts of TNF and NFKBIs in PRRSV-infected PAMs cultured *ex vivo*. PAMs were harvested from PRRSV-free pigs and cultured in Lab-Tek chambers. The cells were infected with FL12-GFP at a multiplicity of infection of 0.1 $TCID_{50}$ per cell. At various time points p.i., cells were fixed and processed for *in situ* hybridization using probe specific to PRRSV, NFKBIA, NFKBIZ, TNFAIP3, and TNF. Hybridization signal was revealed using the RNAscope 2.5 HD red detection kit. Bar = 50 μm.

Detection of TNF and NFKBI transcripts in lung sections of PRRS-infected pigs. *In situ* hybridization was also used to examine the expression of the PRRSV genome and the 4 selected host genes in the lung sections from PRRSV-infected pigs. $PRRSV^+$ cells were detected at 1 dpi and increased significantly at 3 and 8 dpi. At 15 dpi, the frequency of $PRRSV^+$ cells decreased significantly, and only a few infected cells were detected (Fig. 7).

Among the 4 host genes tested, NFKBIA displayed the strongest staining signal, which was widely distributed throughout various components of the tissue, including alveolar septa, bronchiolar and glandular epithelium, and endothelium (Fig. 7). Even though basal expression level of NFKBIA was observed in lung sections of mock-infected pigs, the staining signal and the frequency of cells labeled with NFKBIA probe was much more prominent in lung sections collected from PRRSV-infected pigs. The staining intensity of NFKBIA was highest at 3 dpi and slightly reduced at 8 and 15 dpi.

Different from NFKBIA, the NFKBIZ staining signal was overall broncho/bronchiolar centered, with the lining epithelium staining darkly the entire circumference of several airways, particularly at later time points of infection. Staining signal was observed at 1 dpi and remained until 15 dpi (Fig. 7).

The staining patterns for TNF and TNFAIP3 probes were similar, with staining signal mainly observed in alveolar septa (Fig. 7). Based on position and morphology of cells with the counterstain, many, if not the majority, of TNF- and TNFAIP3-positive cells appeared to be macrophages. The endothelium staining was very subtle where it occurred and relatively insignificant compared to the frequency and intensity of staining in the alveolar septa. The frequency of cells expressing TNF and TNFAIP3 was

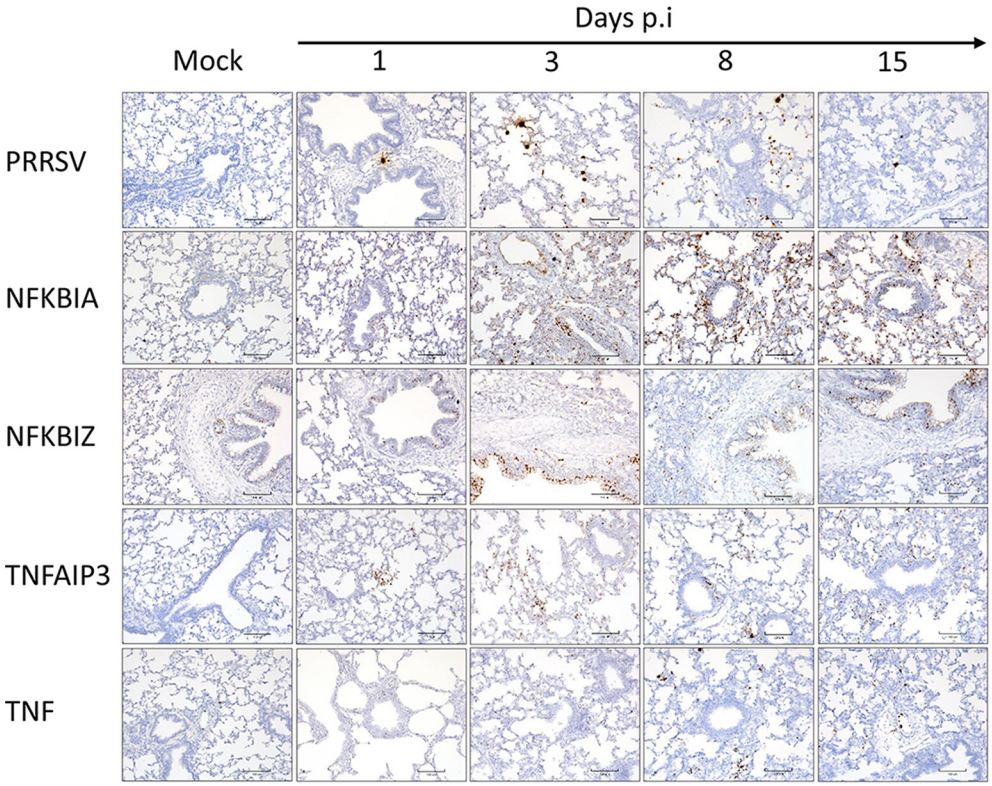

FIG 7 Detection of RNA transcripts of TNF and NFKBIs in lung sections of PRRSV-infected pigs. Lung tissue samples were collected from FL12-infected pigs at 1, 3, 8, and 15 dpi (Materials and Methods, pig experiment 1). ISH was performed using probe specific to PRRSV, NFKBIA, NFKBIZ, TNFAIP3, and TNF. Hybridization signal was detected using the RNAscope 2.5 HD brown detection kit. Bar = 100 μm.

significantly lower than that of NFKIBA and NFKBIZ. TNFAIP3-positive cells appeared at 3 dpi, while TNF-positive cells were observed at 8 dpi. For TNFAIP3, the distribution of staining was remarkably sparse in mock-infected animals at 8 dpi compared to their infected counterparts. TNF signal was most widespread and intense in infected animals at 8 and 15 dpi.

Increased expression of T-cell exhaustion markers in PRRSV-infected PAMs. In addition to the NF-κB signaling pathway, the T-cell exhaustion pathway was also enriched and activated in GFP$^+$ PAMs. Multiple genes involved in the induction of T-cell exhaustion were significantly upregulated in the mock versus GFP$^+$ comparison (Fig. 8A). Notably, PD-L1 (CD274) and PD-L2 (PDCD1LG2), the two immune suppressive transmembrane proteins that interact with the PD1 receptor on T cells and drive T cells into a state of exhaustion, were upregulated in GFP$^+$ cells (Fig. 8B). Expression of the immune suppressive cytokines IDO1, IL-10, and TGFB2 was upregulated in GFP$^+$ PAMs (Fig. 8B). Additionally, expression of several genes in the IFN-STAT1-IRF1 axis which are involved in the upregulation of PD-L1 expression on antigen-presenting cells was significantly upregulated in GFP$^+$ cells. Collectively, these results suggest that GFP$^+$ PAMs displayed coordinated upregulation of several genes associated with T-cell exhaustion.

DISCUSSION

PRRSV has a narrow tropism for cells of the monocyte/macrophage linage (21). PRRSV antigens can be detected in lung and various lymphoid organs of infected pigs (2). By using immunohistochemistry staining of lung sections from pigs infected with a PRRSV-1 isolate, it was reported that no more than 2% of PAMs in the sections harbored viral antigens (2). In the current study, by using flow cytometry analysis of PAMs collected from pigs infected with a PRRSV-2 isolate, we identified that the highest frequency of PRRSV$^+$ PAM was 1.01%. The frequency of PRRSV$^+$ PAMs was highest at

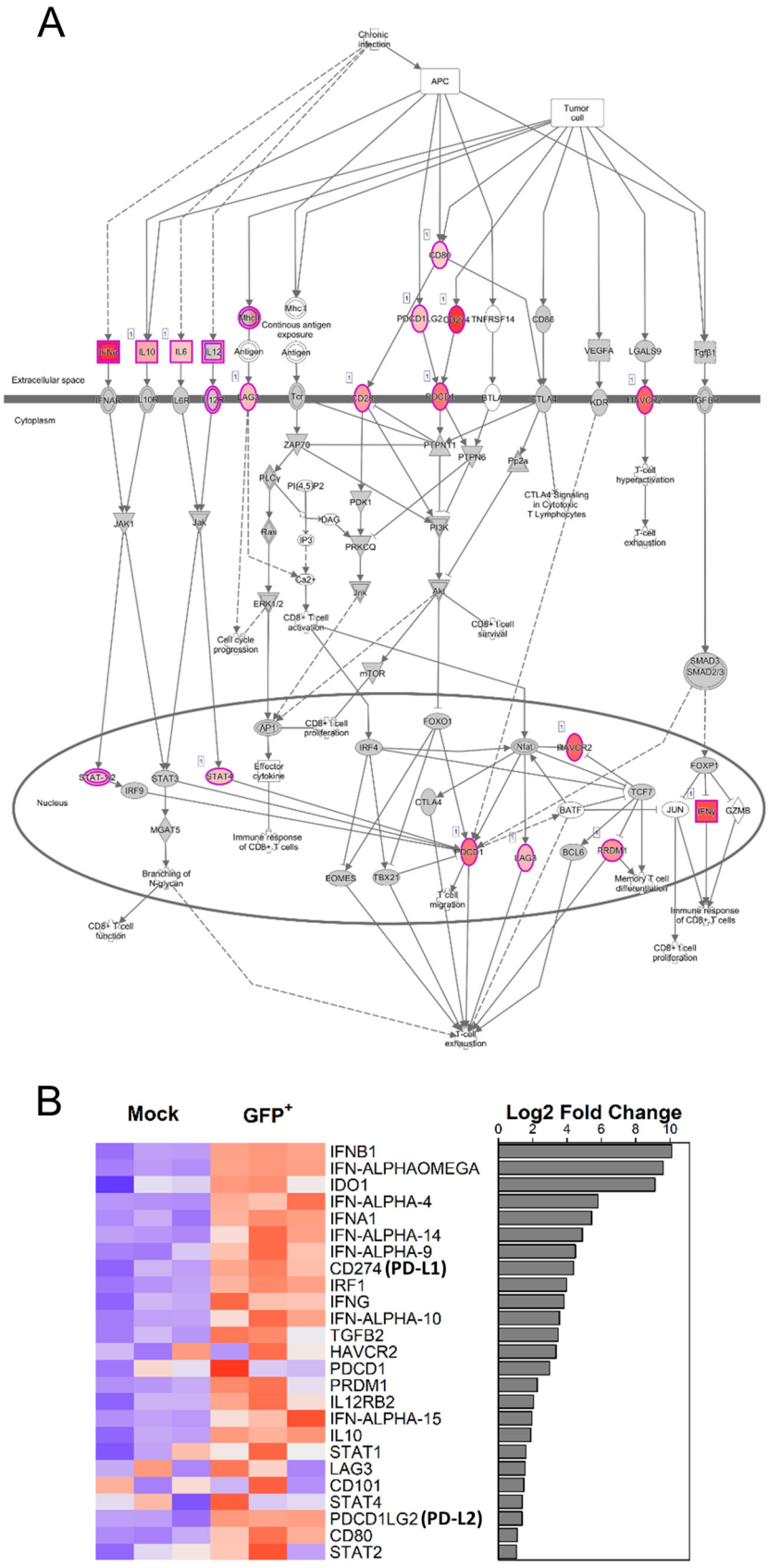

FIG 8 Activation of the T-cell exhaustion pathway in PRRSV-infected PAMs. (A) Pathway image from IPA illustrating genes associated with the T-cell exhaustion signaling pathway using DEGs from the mock versus

(Continued on next page)

8 dpi and declined to a minimal level at 15 dpi. Thus, our results corroborate the previous finding that PRRSV infects only a small fraction of PAMs from PRRSV-infected pigs during the acute stage of infection. PAMs collected from young pigs were more susceptible to *ex vivo* infection with PRRSV than those collected from adult pigs (22). In the current study, pigs were inoculated with PRRSV when they were 4 weeks old. At this age, their PAMs are supposed to be highly susceptible to PRRSV infection (22). Therefore, the low frequency of PRRSV$^+$ PAMs from the BALF of PRRSV-infected pigs observed in this study was not likely due to the refractory stage of the cells to PRRSV infection. Sialoadhesin (CD169) and CD163 are the two main cellular receptors for PRRSV entry into porcine macrophages (reviewed in reference 23). We did not analyze the expression of sialoadhesin because this receptor is not required for PRRSV infection *in vivo* (24). On the other hand, we observed that more than 90% of PAMs expressed CD163 (Fig. 1), the cellular receptor for PRRSV infection (19). Thus, the low frequencies of PRRSV+ PAMs were not likely due to the lack of cellular receptors either. It has been suggested that the origin and state of differentiation and activation affects the susceptibility of porcine macrophages to PRRSV infection. PAMs after 1 day of cultivation *ex vivo* are much more susceptible to PRRSV infection than freshly isolated PAMs (21). It is possible that the low frequencies of PRRSV$^+$ PAMs from PRRSV-infected pigs could be partially due to the differentiation and activation stage of the PAMs. Additionally, innate immune responses in the lung of infected pigs might also contribute to the inhibition of PRRSV infection of PAMs.

Since only a small fraction of PAMs are directly infected with PRRSV, transcriptome studies using RNA extracted from a whole population of PAMs collected from infected pigs might not reveal the true responses of directly infected cells. In the current study, we therefore inoculated pigs with a PRRSV-GFP strain and sorted directly infected (GFP$^+$) and bystander (GFP$^-$) PAMs from the infected pigs to comparatively analyze transcriptional responses in these two populations. The transcriptional change is much more profound in directly infected than bystander PAMs. We observed several canonical pathways that are only enriched in directly infected PAMs, including T-cell exhaustion signaling, dendritic cell maturation, role of PI3/AKT signaling, HMGB1 signaling, TREM1 signaling, and NF-κB signaling. Of these pathways, we are interested in the NF-κB signaling and T-cell exhaustion pathways, both of which contain molecules that negatively regulate the immune responses by modulating inflammation.

PRRSV infection induces inflammatory responses, leading to the infiltration of immune cells (11). High levels of inflammatory cytokines such as IL-1α, IL-6, IL-8 (CXCL8), and TNF have been detected in PRRSV-infected pigs, especially those that are infected with highly virulent PRRSV strains (25–27). Overinduction of proinflammatory cytokines contributes to the manifestation of severe lung damage in pigs infected with a highly virulent PRRSV strain (26, 27). In agreement with previous studies, we observed in this study the upregulation of multiple inflammatory genes in directly infected PAMs, including TNF, CCL4, IL-1B, CXCL8, IL-1A, CCL5, and CXCL10. Notably, several genes that function as negative regulators of cytokine signaling pathways are also highly upregulated in PRRSV-infected PAMs, including suppressor of cytokine signaling (SOCS) proteins (SOCS1 and SOCS3), TNFAIP3, and the inhibitors of NF-κB proteins (NFKBIA, NFKBID, and NFKBIZ). SOCS proteins are inhibitors of the JAK/STAT signaling pathways. In particular, SOCS1 is a ubiquitin ligase which regulates NF-κB signaling and terminates expression of NF-κB inducible genes through polyubiquitination and proteasomal degradation of nuclear p65, a member of the NF-κB (28). TNFAIP3 is a ubiquitin-modifying enzyme that has both ubiquitin ligase and deubiquitinase activities. It removes K63-polyubiquitin

FIG 8 Legend (Continued)
GFP$^+$ comparison. Red color indicates the genes that are upregulated in this comparison. Nondifferentially expressed genes within the pathway are depicted in gray. (B) Heatmap showing the genes that are upregulated in the mock versus GFP$^+$ comparison and associated to develop the T-cell exhaustion phenotype. Bar graphs represent the $\log_2$ fold change of the T-cell exhaustion pathway transcripts.

chains from receptor interacting protein 1 (RIP1) and NF-κB essential modulator (NEMO) while adding K48-polyubiquitin chains to RIP1 and Ubc13, leading to their degradation and, consequently, termination of NF-κB activation (29). NFKBIA, NFKBID, and NFKBIZ belong to a family of proteins called inhibitors of NF-κB, or IκB proteins, which interact with NF-κB dimers to hold them in an inactive form in the cytosol (30, 31). Degradation of these IκBs upon their phosphorylation by the IκB kinase (IKK) releases NF-κB, which is translocated into the nucleus to stimulate expression of inflammatory cytokines and other genes (30). Collectively, the upregulation of both pro- and anti-inflammatory genes within directly infected PAMs reflects the dynamic changes in the host innate immune response to acute PRRSV infection.

As discussed above, pigs infected with a highly virulent PRRSV strain produce high levels of proinflammatory cytokines, which leads to severe lung damage (26, 27). On the other hand, pigs infected with a highly virulent PRRSV strain clear the virus from their tissues much earlier than those infected with a low-virulence PRRSV strain, partially due to the induction of inflammation (26). Therefore, inflammation is critical for effective host defense, but excessive inflammation might be detrimental to the host. Thus, the inflammatory response is tightly controlled by several feedback mechanisms (32). There are two plausible explanations for the upregulation of the negative regulatory genes observed in PRRSV-infected PAMs. It is possible that the expression of the regulatory genes was simply the consequence of the expression of inflammatory cytokines which are triggered by double-stranded RNA (dsRNA) intermediates formed during the viral genome replication. Alternatively, it is possible that PRRSV actively induces expression of the negative regulatory proteins to suppress inflammation and other innate immune responses. The current literature seems to support the latter explanation. PRRSV infection activates expression of SOCS1 and SOCS3, leading to suppression of IFN expression while enhancing virus replication (8, 33). The viral nsp2 carries an OTU domain that inhibits NF-κB activation by interfering with the polyubiqutination and degradation of IκBα (3). Additionally, nsp2 upregulates expression of TREM2, an anti-inflammatory receptor, to suppress inflammatory cytokine production (34). Several viruses have evolved strategies to suppress NF-κB activation. Vaccinia virus A49 protein harbors a sequence mimicking IκBα to block the action of the B-TrCP E3 ligase responsible for identification and ubiquitination of phosphorylated IκBs, thus inhibiting NF-κB activation (35). The nonstructural protein 1 of human rotavirus induces the degradation of B-TrCP to stabilize the IκBs and avoid NF-κB activation (36).

In addition to the NF-κB signaling pathway, the T-cell exhaustion pathway was also exclusively activated in the PRRSV-infected PAMs. In particular, multiple T-cell exhaustion/impairment markers, including PD-L1, PD-L2, IL-10, IDO1, TGFB, CCL2, and PRDM1, were upregulated in PRRSV-infected PAMs. PD-L1 and PD-L2 are the two ligands for PD-1, an inhibitory receptor induced in activated T cells. Engagement of PD-L1 and PD-L2 with PD-1 inhibits the T-cell receptor (TCR) signaling pathway, leading to inhibition of T-cell proliferation and cytokine production (37). Initially, the PD-L1/PD-1 signaling pathways were mainly described in chronic infections and cancer (38, 39). However, it has been subsequently demonstrated that acute viral respiratory infection could rapidly induce $CD8^+$ T-cell impairment (40). For the viruses that mainly replicate in lung, such as human metapneumovirus (HMPV), T-cell impairment during the acute stage of infection mainly occurs in lung, the infection site, while virus-specific T cells in other tissues, such as spleen, are completely functional (41). Unlike HMPV, which mainly replicates in lung and causes acute infection, PRRSV can establish a systemic infection in which the virus can replicate in multiple tissues, including lung and lymphoid organs (2). Moreover, PRRSV can persist in the infected animal for a long period of time (42). Increased expression levels of PD-L1 and several other immune checkpoints, including CTLA4, TIM3, LAG3, CD200R1 and IDO1, were detected in thymus of pigs infected with PRRSV-1 strains during the acute stage of infection (43). Similarly, expression of multiple genes involved in the T-cell exhaustion pathway, including PD-1, IDO1, HAVCR2, and FAS, were also upregulated in the inguinal lymph node of pigs persistently

infected with a PRRSV-2 strain (44). *In vitro* studies have shown that some strains of PRRSV-2 induce expression of PD-L1 in monocyte-derived dendritic cells, especially when the cells were coinfected with porcine circovirus type 2 (9, 45). Collectively, the current literature suggests that PRRSV might induce T-cell impairment in different tissues. While upregulation of T-cell exhaustion markers has been reported previously both *in vivo* and *ex vivo* infection studies, it remains unknown how PRRSV induces T-cell exhaustion. In this study, we observed that T-cell exhaustion markers were only upregulated in directly infected PAMs, not in bystander PAMs. Therefore, it is possible that active viral replication is necessary for the induction of T-cell exhaustion markers. However, the viral genes associated with this process remain to be determined.

In summary, by comparing the transcriptome profiles between PRRSV-infected and bystander PAMs collected from PRRSV pigs during the acute stage of infection, we detected the upregulated expression of multiple negative regulatory genes, including genes that are involved in suppression of inflammation and those that are involved in T-cell impairment. Upregulation of the negative regulatory genes in PRRSV-infected PAMs might help prevent excessive inflammation and protect the lung from immune-mediated damage (46). However, it would be possible that suppression of inflammatory cytokines in lung would enhance PRRSV infection since inflammatory factors downregulate expression of CD163, the main receptor for PRRSV infection, leading to reduction of PRRSV infection (34). Additionally, upregulation of the negative regulators and T-cell exhaustion markers during the acute stage of infection might lead to suboptimal induction of the adaptive immunity, which might help the virus establish persistent infection in the infected animals.

MATERIALS AND METHODS

Cells, viruses, and antibodies. MARC-145 cells were cultured in low-glucose Dulbecco modified Eagle medium (DMEM) supplemented with 10% fetal bovine serum (FBS), 100 units/ml of penicillin, and 100 μg/ml of streptomycin (Sigma-Aldrich, St. Louis, MO). PAMs used for *ex vivo* infection were harvested from lung lavage fluid of PRRSV-negative pigs between 4 and 8 weeks old. The cells were cryopreserved in freezing medium containing 50% RPMI 1640, 40% FBS, and 10% dimethyl sulfoxide (DMSO) and stored in liquid nitrogen until they were used. The PRRSV strains FL12 and FL12-GFP were recovered from full-length infectious cDNA clones as previously described (47, 48). The FL12-GFP carries the GFP gene at the junction between open reading frames 1b and 2a. R-phycoerythrin (R-PE) conjugated mouse anti-pig CD163 monoclonal antibody (clone 2A10/11) was purchased from Bio-Rad (Hercules, CA). Fluorescein (FITC) conjugated mouse anti-PRRSV N protein antibody (clone SR30) was purchased from Rural Tech, Inc. (RTI; Brookings, SD).

Animal studies. All pig experiments conducted in this study were approved by the Institutional Animal Care Committee of the University of Nebraska-Lincoln (UNL) under protocol 1873. All pigs used in this study were between 4 and 5 weeks of age and were free of PRRSV. The pigs were accommodated in the animal biosafety level 2 (ABSL-2) research facility at UNL. Two pig experiments were conducted. In the first experiment, 12 pigs were housed in a single ABSL-2 room and were inoculated intramuscularly with $10^{5.0}$ 50% tissue culture infective dose ($TCID_{50}$) of PRRSV strain FL12 diluted in 2 ml of DMEM. Whole-blood samples were collected, and serum was isolated and stored at −70°C for measurement of viral loads in serum. At 1, 3, 8, and 15 dpi, three pigs were randomly selected and humanely euthanized by overdose of pentobarbital sodium (Virbac, Fort Worth, TX). Lung lavage fluid was collected using ice-cold 1× phosphate-buffered saline (PBS) and processed for flow cytometry analysis to determine the frequencies of PAM infected with PRRSV (described in the next section). Simultaneously, samples of lung were collected and fixed in 10% neutral buffered formalin (NBF) for 24 to 30 h at room temperature (RT), which were used for ISH staining. In the second experiment, 6 pigs were randomly assigned into two groups of three pigs, which were accommodated in two separate ABSL-2 rooms. Pigs in group 1 were injected with RPMI 1640 to serve as negative controls, whereas pigs in group 2 were inoculated with $10^{6.0}$ $TCID_{50}$/ml of FL12-GFP diluted in 4 ml of RPMI 1640—2 ml intramuscularly and 2 ml intranasally. At 7 dpi, all pigs were humanely euthanized by overdose of pentobarbital sodium (Virbac). Lung lavage fluid from each pig was harvested and process for cell sorting. Lung tissue was also collected and processed as described above for ISH staining.

Flow cytometry and PAM cell sorting. PAM cells were suspended in FACS buffer (PBS with 4% FBS). For experiment 1, approximately 1 million cells were first incubated with Zombie Violet live-dead fixable dye (BioLegend, San Diego, CA) (dilution, 1:100 in PBS) at room temperature in the dark for 20 min. Cells were washed thrice using FACS buffer and incubated with R-PE labeled, anti-pig CD163 antibody (dilution, 1:50 in FACS buffer) on ice in the dark for 30 min. After three washes in FACS buffer, the cells were fixed and permeabilized with 4% paraformaldehyde and Leucoperm buffer (Bio-Rad, Hercules, CA), respectively. Subsequently, the cells were incubated with FITC conjugated, anti-PRRSV N protein antibody (dilution, 1:100 in FACS buffer) for 30 min. After three washes with FACS buffer,

the cells were analyzed by using a CytoFlex cytometer (Beckman Coulter, Fremont, CA). Approximately 30,000 events were recorded for each sample. Data were analyzed using FlowJo software (BD Biosciences, San Jose, CA).

In experiment 2, PAMs were stained with R-PE labeled anti-pig CD163 antibody as described above. Without fixation and permeabilization, the cells were subjected to FACS analysis using a FACSAria instrument (BD Biosciences, San Jose, CA). Three populations of PAMs were sorted, $CD163^+$ from mock-infected pigs, $CD163^+GFP^+$, and $CD163^+GFP^-$ from FL12-GFP infected pigs. Approximately 40,000 PAMs were sorted for each of the above-mentioned populations. Sorted PAMs was lysed in 50 μl of TRIzol reagent (Life Technologies, Carlsbad, CA) and subjected to RNA sequencing (RNA-seq).

PAM cell RNA extraction, library preparation, and sequencing. RNA-seq was performed through a contract service with Genewiz LLC (Carol Stream, IL) with the ultra-low input RNA sequencing package. Briefly, total RNA was extracted and quantified using a Qubit fluorometer (Life Technologies, Carlsbad, CA). RNA integrity was checked with TapeStation (Agilent Technologies, Palo Alto, CA). Only RNA samples with an RNA integrity number (RIN) equal to or above 8.0 were included in this study. The SMART-Seq v4 ultra-low input kit for sequencing was used for full-length cDNA synthesis and amplification (Clontech, Mountain View, CA), and an Illumina Nextera XT library was used for sequencing library preparation. The libraries were multiplexed and clustered on one lane of a flow cell and sequenced using the Illumina HiSeq instrument. The samples were sequenced using a 2 $\times$ 150 paired-end (PE) configuration. Image analysis and base calling were conducted using HiSeq Control Software (HCS). Raw sequence data (.bcl files) generated from the Illumina HiSeq sequencing was converted into FASTQ files and demultiplexed using Illumina's bcl2fastq version 2.17 software. One mismatch was allowed for index sequence identification.

Data processing and analysis. RNA-seq reads were first trimmed with Trim Galore version 0.6.4 (49, 50), which includes filtering reads shorter than 30 bp and low-quality ends from reads (Phred score, $<$20) and the option of removing reads with Ns. The read quality before and after trimming was checked with FastQC version 0.11.7 (51). The filtered reads were aligned to the *Sus scrofa* genome (Sscrofa11.1; GenBank assembly number GCF_000003025.6) using STAR version 2.7.6a (52) with default parameters and –sjdbOverhang of 149. Alignment files generated by STAR were then used to generate gene counts using Subread version 2.0.0 (featureCounts) with default parameters (53). A data matrix of gene counts for all samples was created using a custom Python script, and the data matrix was used to run the differential gene expression analysis in DESeq2 version 1.22.1 (54). Genes with a Benjamini-Hochberg adjusted *P* value smaller than 0.05 and an absolute $\log_2$ fold change larger than 1 were considered differentially expressed. A Wald test was used to determine the DEGs between the $CD163^+$ PAM sorted from mock-infected pigs and $CD163^+GFP^-$ PAM (bystander) and $CD163^+GFP^+$ PAMs sorted from PRRSV-infected pigs. For the pairwise comparison of $CD163^+GFP^-$ and $CD163^+GFP^+$ PAMs sorted from PRRSV-infected pigs, the identity of the pigs was taken into consideration since the PAM cells were collected from the same pigs. The differential expression result table generated by DESeq2 was annotated with gene information obtained from Ensemble BioMart for *Sus scrofa*, supplemented by annotation from the gene transfer format (GTF) file.

To visualize the level of the PRRSV RNA genome, reads mapped to the PRRSV FL12-GFP genome were counted base by base, normalized to counts per million, and subsequently used to generate a coverage track using deepTools version 3.4.3 (55).

Differentially expressed genes were used for the significant canonical pathway and molecular network identification using Ingenuity pathway analysis (IPA; Qiagen, Redwood City, CA). The pathway enrichment *P* value (Fisher's exact test) and activation Z-score were calculated using IPA and used to rank the significant pathways.

PRRSV infection of PAM cultured *ex vivo*. Cryopreserved PAMs were revived and cultured in RPMI 1640 supplemented 10% FBS in a 4-chambered Lab-Tek slide (Nunc, Rochester, NY) at a density of 5×10^5 cells in 1 ml per chamber. After 24 h, the cells were either mock-infected or infected with FL12-GFP at a multiplicity of infection of 0.1 $TCID_{50}$ per cell. At 6, 12, and 18 h postinfection (hpi), the cells were fixed using 10% NBF for 30 min at room temperature and subsequently used for ISH staining.

RNA *in situ* hybridization. ISH was used to detect mRNA transcripts of PRRSV, NFKBIA, NFKBIZ, TNFAIP3, and TNF, both in formalin-fixed paraffin-embedded (FFPE) lung sections and in PAMs infected with PRRSV *ex vivo*. ISH was performed using the RNAscope technology. Specific probes for PRRSV (catalog [cat.] no. 870971), NFKBIA (cat. no. 867461), NFKBIZ (cat. no. 867441), TNFAIP3 (cat. no. 867451), and TNF (cat. no. 565841) were developed by Advanced Cell Diagnostics (ACD, Hayward, CA). The probes were supplied in a ready-to-use format. Probes specific to dihydrodipicolinate reductase B (dapB) (cat. no. 310043) mRNA of *Bacillus subtilis* and *Sus Scrofa* peptidylprolyl isomerase B (Ss-PPIB) (cat. no. 428591) were used as negative and positive controls, respectively. The RNAscope 2.5 HD brown detection kit (ACD) was used for ISH assays that were done on FFPE lung tissue, while the RNAscope 2.5 HD red detection kit was used for assays that were done with PAM cultured *ex vivo* on a Lab-Tek slide.

The ISH assay performed on FFPE lung was qualitatively assessed by a board-certified pathologist who was blinded to the experimental treatment groups. Two main parameters were used to evaluate ISH signal, the intensity of staining signal and the frequency (distribution) of stained cells throughout the section.

Measurement of viral load and serum virus titer. Total RNA was extracted from serum samples using a viral RNA minikit (Qiagen GmbH, Hilden, Germany) following the manufacturer's recommendation. Viral load in serum was measured using a commercial reverse transcriptase quantitative PCR (RT-qPCR) kit (Tetracore, Inc., Rockville, MD, USA) and was reported as $\log_{10}$ copies per ml of total RNA used

in the RT-qPCR. For statistical purposes, samples that had no detectable levels of viral RNA were assigned a value of 0 $\log_{10}$ copies.

Data availability. The RNA-seq data were deposited in the Gene Expression Omnibus (GEO) under accession number GSE174494.

ACKNOWLEDGMENTS

This study was funded by the Agriculture and Food Research Initiative competitive grants 2018-67015-28294 and the Multi-state Hatch project 1020749 of the USDA National Institute for Food and Agriculture.

We thank Dirk Anderson at the Flowcytometry Core Facility, Nebraska Center for Biotechnology, for his assistance with the flow cytometry and cell sorting and Lorena Bustamante-Cordova for her assistance with PAM cell isolation. We also thank the staff members of UNL Life Sciences Annex and Veterinary Diagnostic Center for the care of animals.

REFERENCES

1. Brinton MA, Gulyaeva AA, Balasuriya UBR, Dunowska M, Faaberg KS, Goldberg T, Leung FCC, Nauwynck HJ, Snijder EJ, Stadejek T, Gorbalenya AE. 2021. ICTV virus taxonomy profile: Arteriviridae. J Gen Virol) 102. https://doi.org/10.1099/jgv.0.001632.
2. Duan X, Nauwynck HJ, Pensaert MB. 1997. Virus quantification and identification of cellular targets in the lungs and lymphoid tissues of pigs at different time intervals after inoculation with porcine reproductive and respiratory syndrome virus (PRRSV). Vet Microbiol 56:9–19. https://doi.org/10.1016/S0378-1135(96)01347-8.
3. Sun Z, Chen Z, Lawson SR, Fang Y. 2010. The cysteine protease domain of porcine reproductive and respiratory syndrome virus nonstructural protein 2 possesses deubiquitinating and interferon antagonism functions. J Virol 84:7832–7846. https://doi.org/10.1128/JVI.00217-10.
4. Beura LK, Sarkar SN, Kwon B, Subramaniam S, Jones C, Pattnaik AK, Osorio FA. 2010. Porcine reproductive and respiratory syndrome virus nonstructural protein 1beta modulates host innate immune response by antagonizing IRF3 activation. J Virol 84:1574–1584. https://doi.org/10.1128/JVI.01326-09.
5. Patel D, Nan Y, Shen M, Ritthipichai K, Zhu X, Zhang YJ. 2010. Porcine reproductive and respiratory syndrome virus inhibits type I interferon signaling by blocking STAT1/STAT2 nuclear translocation. J Virol 84:11045–11055. https://doi.org/10.1128/JVI.00655-10.
6. Song C, Krell P, Yoo D. 2010. Nonstructural protein 1alpha subunit-based inhibition of NF-kappaB activation and suppression of interferon-beta production by porcine reproductive and respiratory syndrome virus. Virology 407:268–280. https://doi.org/10.1016/j.virol.2010.08.025.
7. Subramaniam S, Kwon B, Beura LK, Kuszynski CA, Pattnaik AK, Osorio FA. 2010. Porcine reproductive and respiratory syndrome virus non-structural protein 1 suppresses tumor necrosis factor-alpha promoter activation by inhibiting NF-kappaB and Sp1. Virology 406:270–279. https://doi.org/10.1016/j.virol.2010.07.016.
8. Luo X, Chen XX, Qiao S, Li R, Xie S, Zhou X, Deng R, Zhou EM, Zhang G. 2020. Porcine reproductive and respiratory syndrome virus enhances self-replication via AP-1-dependent induction of SOCS1. J Immunol 204:394–407. https://doi.org/10.4049/jimmunol.1900731.
9. Richmond O, Cecere TE, Erdogan E, Meng XJ, Pineyro P, Subramaniam S, Todd SM, LeRoith T. 2015. PD-L1 expression is increased in monocyte derived dendritic cells in response to porcine circovirus type 2 and porcine reproductive and respiratory syndrome virus infections. Vet Immunol Immunopathol 168:24–29. https://doi.org/10.1016/j.vetimm.2015.09.013.
10. Islam MA, Neuhoff C, Aqter Rony S, Große-Brinkhaus C, Uddin MJ, Hölker M, Tesfaye D, Tholen E, Schellander K, Pröll-Cornelissen MJ. 2019. PBMCs transcriptome profiles identified breed-specific transcriptome signatures for PRRSV vaccination in German Landrace and Pietrain pigs. PLoS One 14:e0222513. https://doi.org/10.1371/journal.pone.0222513.
11. Xiao S, Mo D, Wang Q, Jia J, Qin L, Yu X, Niu Y, Zhao X, Liu X, Chen Y. 2010. Aberrant host immune response induced by highly virulent PRRSV identified by digital gene expression tag profiling. BMC Genomics 11:544. https://doi.org/10.1186/1471-2164-11-544.
12. Zhou P, Zhai S, Zhou X, Lin P, Jiang T, Hu X, Jiang Y, Wu B, Zhang Q, Xu X, Li JP, Liu B. 2011. Molecular characterization of transcriptome-wide interactions between highly pathogenic porcine reproductive and respiratory syndrome virus and porcine alveolar macrophages in vivo. Int J Biol Sci 7:947–959. https://doi.org/10.7150/ijbs.7.947.
13. Miller LC, Fleming D, Arbogast A, Bayles DO, Guo B, Lager KM, Henningson JN, Schlink SN, Yang HC, Faaberg KS, Kehrli ME Jr. 2012. Analysis of the swine tracheobronchial lymph node transcriptomic response to infection with a Chinese highly pathogenic strain of porcine reproductive and respiratory syndrome virus. BMC Vet Res 8:208. https://doi.org/10.1186/1746-6148-8-208.
14. Crisci E, Moroldo M, Vu Manh TP, Mohammad A, Jourdren L, Urien C, Bouguyon E, Bordet E, Bevilacqua C, Bourge M, Pezant J, Pleau A, Boulesteix O, Schwartz I, Bertho N, Giuffra E. 2020. Distinctive cellular and metabolic reprogramming in porcine lung mononuclear phagocytes infected with type 1 PRRSV strains. Front Immunol 11:588411. https://doi.org/10.3389/fimmu.2020.588411.
15. Badaoui B, Rutigliano T, Anselmo A, Vanhee M, Nauwynck H, Giuffra E, Botti S. 2014. RNA-sequence analysis of primary alveolar macrophages after in vitro infection with porcine reproductive and respiratory syndrome virus strains of differing virulence. PLoS One 9:e91918. https://doi.org/10.1371/journal.pone.0091918.
16. Zeng N, Wang C, Liu S, Miao Q, Zhou L, Ge X, Han J, Guo X, Yang H. 2018. Transcriptome analysis reveals dynamic gene expression profiles in porcine alveolar macrophages in response to the Chinese highly pathogenic porcine reproductive and respiratory syndrome virus. Biomed Res Int 2018:1538127. https://doi.org/10.1155/2018/1538127.
17. Genini S, Delputte PL, Malinverni R, Cecere M, Stella A, Nauwynck HJ, Giuffra E. 2008. Genome-wide transcriptional response of primary alveolar macrophages following infection with porcine reproductive and respiratory syndrome virus. J Gen Virol 89:2550–2564. https://doi.org/10.1099/vir.0.2008/003244-0.
18. Badaoui B, Tuggle CK, Hu Z, Reecy JM, Ait-Ali T, Anselmo A, Botti S. 2013. Pig immune response to general stimulus and to porcine reproductive and respiratory syndrome virus infection: a meta-analysis approach. BMC Genomics 14:220. https://doi.org/10.1186/1471-2164-14-220.
19. Calvert JG, Slade DE, Shields SL, Jolie R, Mannan RM, Ankenbauer RG, Welch SK. 2007. CD163 expression confers susceptibility to porcine reproductive and respiratory syndrome viruses. J Virol 81:7371–7379. https://doi.org/10.1128/JVI.00513-07.
20. Li Q, Verma IM. 2002. NF-kappaB regulation in the immune system. Nat Rev Immunol 2:725–734. https://doi.org/10.1038/nri910.
21. Duan X, Nauwynck HJ, Pensaert MB. 1997. Effects of origin and state of differentiation and activation of monocytes/macrophages on their susceptibility to porcine reproductive and respiratory syndrome virus (PRRSV). Arch Virol 142:2483–2497. https://doi.org/10.1007/s007050050256.
22. Gray DK, Dvorak CMT, Robinson SR, Murtaugh MP. 2019. Characterization of age-related susceptibility of macrophages to porcine reproductive and respiratory syndrome virus. Virus Res 263:139–144. https://doi.org/10.1016/j.virusres.2019.01.015.
23. Van Breedam W, Delputte PL, Van Gorp H, Misinzo G, Vanderheijden N, Duan X, Nauwynck HJ. 2010. Porcine reproductive and respiratory syndrome virus entry into the porcine macrophage. J Gen Virol 91:1659–1667. https://doi.org/10.1099/vir.0.020503-0.
24. Prather RS, Rowland RR, Ewen C, Trible B, Kerrigan M, Bawa B, Teson JM, Mao J, Lee K, Samuel MS, Whitworth KM, Murphy CN, Egen T, Green JA. 2013. An intact sialoadhesin (Sn/SIGLEC1/CD169) is not required for attachment/internalization of the porcine reproductive and respiratory syndrome virus. J Virol 87:9538–9546. https://doi.org/10.1128/JVI.00177-13.

25. Liu Y, Shi W, Zhou E, Wang S, Hu S, Cai X, Rong F, Wu J, Xu M, Xu M, Li L. 2010. Dynamic changes in inflammatory cytokines in pigs infected with highly pathogenic porcine reproductive and respiratory syndrome virus. Clin Vaccine Immunol 17:1439–1445. https://doi.org/10.1128/CVI.00517-09.
26. Weesendorp E, Rebel JM, Popma-De Graaf DJ, Fijten HP, Stockhofe-Zurwieden N. 2014. Lung pathogenicity of European genotype 3 strain porcine reproductive and respiratory syndrome virus (PRRSV) differs from that of subtype 1 strains. Vet Microbiol 174:127–138. https://doi.org/10.1016/j.vetmic.2014.09.010.
27. Amarilla SP, Gomez-Laguna J, Carrasco L, Rodriguez-Gomez IM, Caridad YOJM, Morgan SB, Graham SP, Frossard JP, Drew TW, Salguero FJ. 2015. A comparative study of the local cytokine response in the lungs of pigs experimentally infected with different PRRSV-1 strains: upregulation of IL-1alpha in highly pathogenic strain induced lesions. Vet Immunol Immunopathol 164:137–147. https://doi.org/10.1016/j.vetimm.2015.02.003.
28. Strebovsky J, Walker P, Lang R, Dalpke AH. 2011. Suppressor of cytokine signaling 1 (SOCS1) limits NFkappaB signaling by decreasing p65 stability within the cell nucleus. FASEB J 25:863–874. https://doi.org/10.1096/fj.10-170597.
29. Das T, Chen Z, Hendriks RW, Kool M. 2018. A20/tumor necrosis factor alpha-induced protein 3 in immune cells controls development of autoinflammation and autoimmunity: lessons from mouse models. Front Immunol 9:104. https://doi.org/10.3389/fimmu.2018.00104.
30. Oeckinghaus A, Ghosh S. 2009. The NF-kappaB family of transcription factors and its regulation. Cold Spring Harb Perspect Biol 1:a000034. https://doi.org/10.1101/cshperspect.a000034.
31. Yu H, Lin L, Zhang Z, Zhang H, Hu H. 2020. Targeting NF-kappaB pathway for the therapy of diseases: mechanism and clinical study. Signal Transduct Target Ther 5:209. https://doi.org/10.1038/s41392-020-00312-6.
32. Adelaja A, Hoffmann A. 2019. Signaling crosstalk mechanisms that may fine-tune pathogen-responsive NFkappaB. Front Immunol 10:433. https://doi.org/10.3389/fimmu.2019.00433.
33. Luo X, Chen XX, Qiao S, Li R, Lu Q, Geng R, Wang L, Zhou EM, Zhang G. 2021. Porcine reproductive and respiratory syndrome virus increases SOCS3 production via activation of p38/AP-1 signaling pathway to promote viral replication. Vet Microbiol 257:109075. https://doi.org/10.1016/j.vetmic.2021.109075.
34. Zhu Z, Zhang X, Dong W, Wang X, He S, Zhang H, Wang X, Wei R, Chen Y, Liu X, Guo C. 2020. TREM2 suppresses the proinflammatory response to facilitate PRRSV infection via PI3K/NF-kappaB signaling. PLoS Pathog 16:e1008543. https://doi.org/10.1371/journal.ppat.1008543.
35. Mansur DS, Maluquer de Motes C, Unterholzner L, Sumner RP, Ferguson BJ, Ren H, Strnadova P, Bowie AG, Smith GL. 2013. Poxvirus targeting of E3 ligase beta-TrCP by molecular mimicry: a mechanism to inhibit NF-kappaB activation and promote immune evasion and virulence. PLoS Pathog 9:e1003183. https://doi.org/10.1371/journal.ppat.1003183.
36. Morelli M, Dennis AF, Patton JT. 2015. Putative E3 ubiquitin ligase of human rotavirus inhibits NF-kappaB activation by using molecular mimicry to target beta-TrCP. mBio 6:e02490-14. https://doi.org/10.1128/mBio.02490-14.
37. Keir ME, Francisco LM, Sharpe AH. 2007. PD-1 and its ligands in T-cell immunity. Curr Opin Immunol 19:309–314. https://doi.org/10.1016/j.coi.2007.04.012.
38. Day CL, Kaufmann DE, Kiepiela P, Brown JA, Moodley ES, Reddy S, Mackey EW, Miller JD, Leslie AJ, DePierres C, Mncube Z, Duraiswamy J, Zhu B, Eichbaum Q, Altfeld M, Wherry EJ, Coovadia HM, Goulder PJ, Klenerman P, Ahmed R, Freeman GJ, Walker BD. 2006. PD-1 expression on HIV-specific T cells is associated with T-cell exhaustion and disease progression. Nature 443:350–354. https://doi.org/10.1038/nature05115.
39. Golden-Mason L, Palmer B, Klarquist J, Mengshol JA, Castelblanco N, Rosen HR. 2007. Upregulation of PD-1 expression on circulating and intrahepatic hepatitis C virus-specific CD8+ T cells associated with reversible immune dysfunction. J Virol 81:9249–9258. https://doi.org/10.1128/JVI.00409-07.
40. Erickson JJ, Lu P, Wen S, Hastings AK, Gilchuk P, Joyce S, Shyr Y, Williams JV. 2015. Acute viral respiratory infection rapidly induces a CD8+ T cell exhaustion-like phenotype. J Immunol 195:4319–4330. https://doi.org/10.4049/jimmunol.1403004.
41. Erickson JJ, Gilchuk P, Hastings AK, Tollefson SJ, Johnson M, Downing MB, Boyd KL, Johnson JE, Kim AS, Joyce S, Williams JV. 2012. Viral acute lower respiratory infections impair CD8+ T cells through PD-1. J Clin Invest 122:2967–2982. https://doi.org/10.1172/JCI62860.
42. Allende R, Laegreid WW, Kutish GF, Galeota JA, Wills RW, Osorio FA. 2000. Porcine reproductive and respiratory syndrome virus: description of persistence in individual pigs upon experimental infection. J Virol 74:10834–10837. https://doi.org/10.1128/jvi.74.22.10834-10837.2000.
43. Ruedas-Torres I, Rodriguez-Gomez IM, Sanchez-Carvajal JM, Guil-Luna S, Larenas-Munoz F, Pallares FJ, Carrasco L, Gomez-Laguna J. 2021. Up-regulation of immune checkpoints in the thymus of PRRSV-1-infected piglets in a virulence-dependent fashion. Front Immunol 12:671743. https://doi.org/10.3389/fimmu.2021.671743.
44. Chaudhari J, Liew CS, Workman AM, Riethoven JM, Steffen D, Sillman S, Vu HLX. 2020. Host transcriptional response to persistent infection with a live-attenuated porcine reproductive and respiratory syndrome virus strain. Viruses 12:817. https://doi.org/10.3390/v12080817.
45. Richmond O, Cecere TE, Erdogan E, Meng XJ, Pineyro P, Subramaniam S, Todd SM, LeRoith T. 2015. The PD-L1/CD86 ratio is increased in dendritic cells co-infected with porcine circovirus type 2 and porcine reproductive and respiratory syndrome virus, and the PD-L1/PD-1 axis is associated with anergy, apoptosis, and the induction of regulatory T-cells in porcine lymphocytes. Vet Microbiol 180:223–229. https://doi.org/10.1016/j.vetmic.2015.09.014.
46. Rogers MC, Williams JV. 2019. Reining in the CD8+ T cell: respiratory virus infection and PD-1-mediated T-cell impairment. PLoS Pathog 15:e1007387. https://doi.org/10.1371/journal.ppat.1007387.
47. Truong HM, Lu Z, Kutish GF, Galeota J, Osorio FA, Pattnaik AK. 2004. A highly pathogenic porcine reproductive and respiratory syndrome virus generated from an infectious cDNA clone retains the in vivo virulence and transmissibility properties of the parental virus. Virology 325:308–319. https://doi.org/10.1016/j.virol.2004.04.046.
48. Beura LK, Dinh PX, Osorio FA, Pattnaik AK. 2011. Cellular poly(C) binding proteins 1 and 2 interact with porcine reproductive and respiratory syndrome virus nonstructural protein 1 beta and support viral replication. J Virol 85:12939–12949. https://doi.org/10.1128/JVI.05177-11.
49. Krueger F. 2019. Trim Galore, GitHub repository, https://github.com/FelixKrueger/TrimGalore. https://doi.org/10.5281/zenodo.5127899.
50. Martin M. 2011. Cutadapt removes adapter sequences from high-throughput sequencing reads. EMBnet J 17:3. https://doi.org/10.14806/ej.17.1.200.
51. Andrews S. 2019. FastQC: a quality control tool for high throughput sequence data. http://www.bioinformatics.babraham.ac.uk/projects/fastqc.
52. Dobin A, Davis CA, Schlesinger F, Drenkow J, Zaleski C, Jha S, Batut P, Chaisson M, Gingeras TR. 2013. STAR: ultrafast universal RNA-seq aligner. Bioinformatics 29:15–21. https://doi.org/10.1093/bioinformatics/bts635.
53. Liao Y, Smyth GK, Shi W. 2014. featureCounts: an efficient general purpose program for assigning sequence reads to genomic features. Bioinformatics 30:923–930. https://doi.org/10.1093/bioinformatics/btt656.
54. Love MI, Huber W, Anders S. 2014. Moderated estimation of fold change and dispersion for RNA-seq data with DESeq2. Genome Biol 15:550. https://doi.org/10.1186/s13059-014-0550-8.
55. Ramirez F, Ryan DP, Gruning B, Bhardwaj V, Kilpert F, Richter AS, Heyne S, Dundar F, Manke T. 2016. deepTools2: a next generation web server for deep-sequencing data analysis. Nucleic Acids Res 44:W160–W165. https://doi.org/10.1093/nar/gkw257.